Journal of Structural Geology, Vol. 13, No. 6, pp. 721 to 733, 1991
Printed in Great Britain

0191-8141/91 $03.00+0.00

Displacements, segment linkage and relay ramps in normal fault zones

D. C. P. PEACOCK and D. J. SANDERSON

Department of Geology, University of Southampton, Southampton SO9 5NH, U.K.

(*Received* 20 *March* 1990; *accepted in revised form* 19 *November* 1990)

Abstract—A fault zone is produced by the displacement and linkage of component segments, and hence these are important to the understanding of fault zone development. A small well-exposed normal fault zone at Kilve, Somerset, U.K., is described, which consists of 34 individual offset and linked fault segments. Antithetic faults appear to be associated with bending at relay ramps and foot wall uplift. A simple model is presented which assumes different displacement gradients inside and outside the influence of relay structures. High displacement gradients at the tips of offset fault segments produce lower r/d_{MAX} ratios than those of isolated faults (where r = distance between the fault tip and point of maximum displacement, and d_{MAX} = maximum displacement). Relay structures form between offset normal fault segments, producing inclined zones (relay ramps) whose geometry can be related to the displacement gradients at the fault tips. Linkage points between segments are marked by fault displacement minima, causing further complexity in displacement–distance data.

INTRODUCTION

FAULT zones result from the displacements along, and the linkage of, component segments. This is clear from the mapping of fault zones (e.g. Walsh & Watterson in press) and the study of seismicity during active fault movement (e.g. King 1983, 1986). Therefore, knowledge of the geometry of fault segments is important in understanding fault zone development. This paper describes the geometry of a small normal fault zone at Kilve, Somerset, U.K. (Fig. 1) which consists of a complex pattern of fault segments. The transfer of displacement from one segment to another occurs through relay structures, whose geometry is determined by the displacement variations along adjacent segments. Linkage of many such segments leads to the final form of the fault zone.

GENERAL DESCRIPTION OF THE FAULT ZONE

The Kilve fault zone is developed in Lower Jurassic rocks; its age is unknown, but it is probably related to the Mesozoic development of the Bristol Channel Basin (Chadwick 1986, Brooks *et al.* 1988, Donato 1988, Beach 1989). Many normal faults in the area show reverse and strike-slip reactivation, caused by Cretaceous or Tertiary compression (McLachlan 1986, Beach 1989), but there is no evidence of reactivation of the fault zone described in this paper.

The fault zone is exposed for a length of approximately 80 m on a gently dipping limestone bed. Maximum vertical displacement is about 400 mm, decreasing to zero at its eastern end, the western tip being covered by overlying shales (Fig. 2). The fault zone consists of

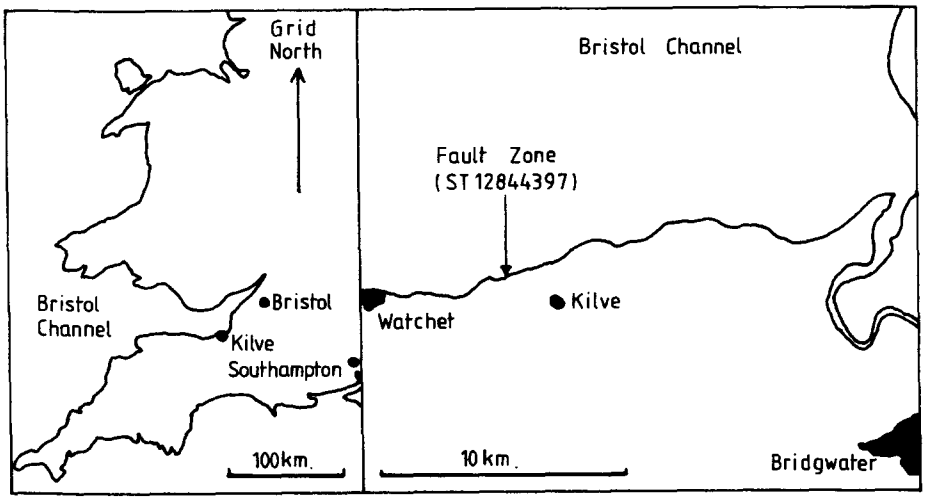

Fig. 1. Location of the Kilve fault zone in Somerset, U.K.

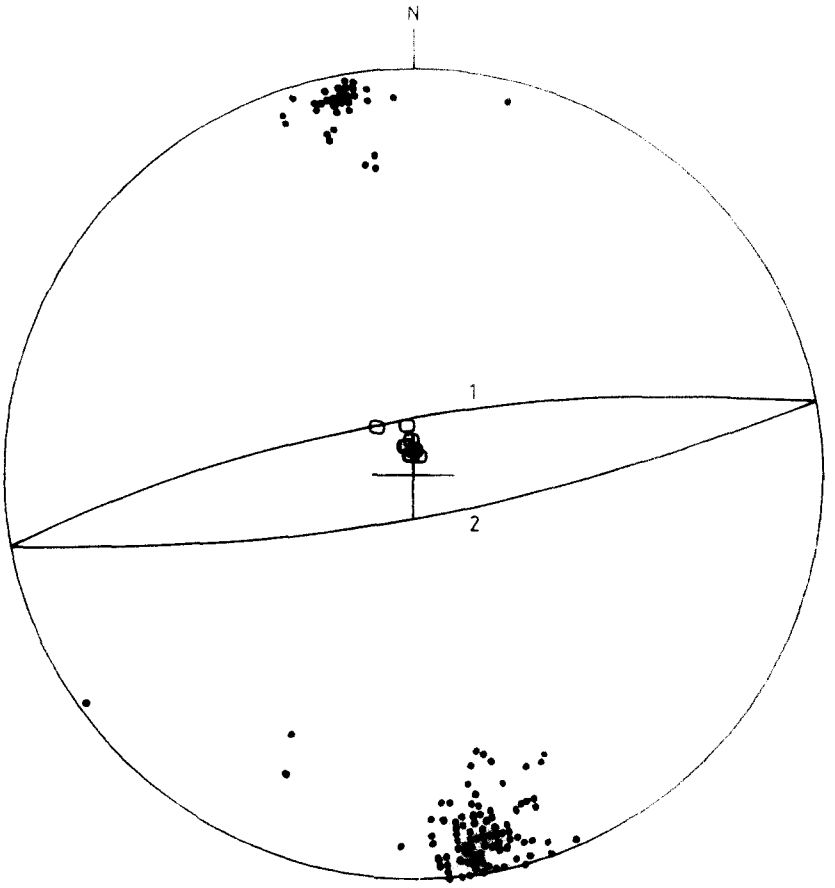

Fig. 3. Stereographic representation of faults in the limestones, and of bedding. Great circles are average dips of faults: 1 = synthetic faults (mean ≈ 80° towards 350°), 2 = antithetic faults (mean ≈ 82° towards 170°). Dots = poles to faults. O = poles to bedding (mean dip ≈ 5° towards 175°).

approximately 22 segments which downthrow to the north (synthetic faults) and 12 which downthrow to the south (antithetic faults). Apart from individual segments being offset, there is a large offset (the *main* offset) towards the centre of the fault zone. Figure 2 was produced using a mosaic of 43 aerial photographs, taken using a camera at the top of a tripod and pole (total height 7.3 m). A rope with markers at 1 m intervals, placed along the length of the fault zone, aided linkage of the photographs. Some distortions occur because of imperfect fit of the photographs. Structure contours for the upper surface of the limestone bed have been produced by use of a surveyors level. Measurement errors, map distortion, interpolation and erosion of the bedding plane account for uncertainties in contours of an estimated ±20 mm. Vertical displacements are accurate to within a few millimetres, errors being due to the irregular nature of the limestone bedding plane, and blanketing by overlying shales in places. The horizontal extension component was measured by adding fault heaves and vein thicknesses, but is probably less accurate due to difficulties in identifying bed cut-offs.

Form of the fault planes, and the development of pull-aparts

Faults either link with other faults or pass into joints and calcite veins. Some smaller faults die out at tips which do not appear to be marked by other structures. Fault planes are mostly well-preserved, with some dip-slip slickensides occurring. In the limestone bed, the synthetic and antithetic faults have average dips of 80° towards 350° and 82° towards 170°, respectively (Fig. 3). Fault planes are marked by calcite veins, which often contain clay probably derived from the shales. This material is developed in pull-aparts, which are common on fault planes at Kilve (Fig. 4). Faults cut the shales at relatively low angles, and are refracted at higher angles through the limestones. As displacement occurs parallel to the fault segments in the shale, a rhomb-shaped pull-apart opens up at the extensional fault bend in the competent bed. This void may be filled by the surrounding shale (Fig. 4), breccia, vein material, or by wall-rock deformation. The pull-aparts decrease the angle between conjugate sets, with the overall fault dip being intermediate between the dips in the shales and limestones.

Reverse drag: structure contours and antithetic faults

The bedding contour pattern indicates a regional dip of about 5° to the south. Most displacement, both for isolated individual fault segments and for the whole fault zone, appears to be accompanied by half-basin type downfolding of the hanging wall rocks (Fig. 2) (cf. Gibson *et al.* 1989, fig. 6b). This is shown by the

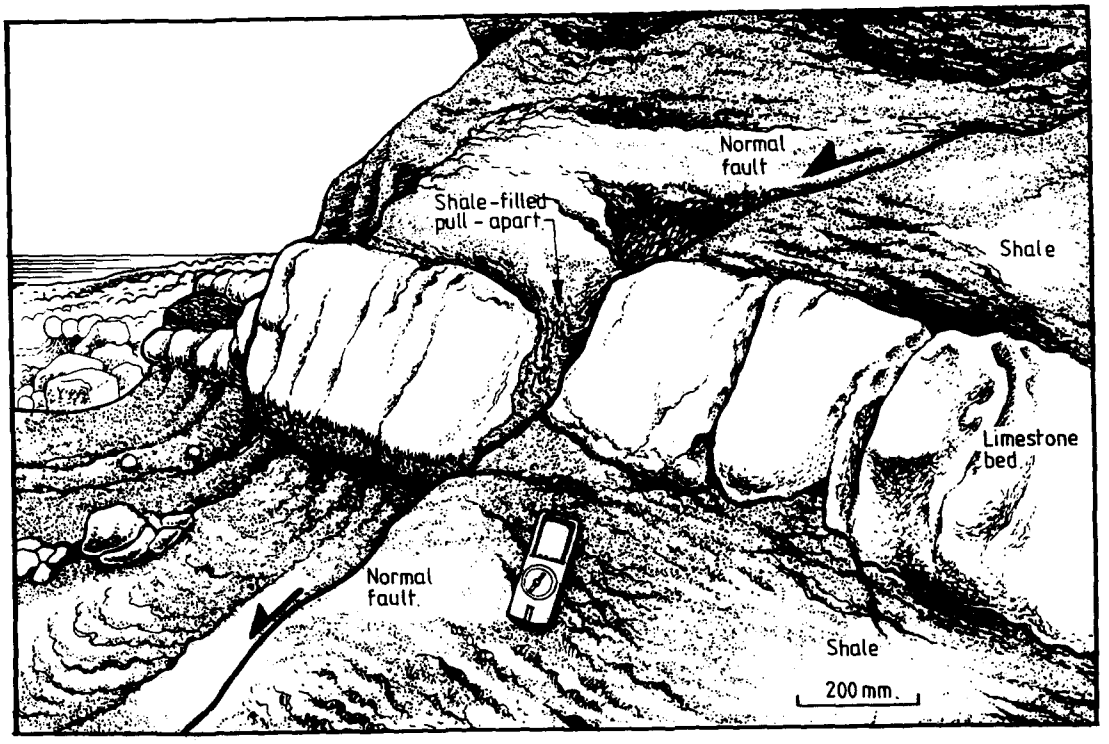

Fig. 4. Line drawing of a pull-apart at grid reference ST13144400, developed by refraction of a fault through a limestone bed. The fault cuts through the limestone bed at a higher angle than in the shales. The effect of pull-aparts is to increase the fault dip and to reduce the angle between conjugate faults. (Drawn by J. Gully.)

approximately straight contours in the foot wall and the strike variability in the hanging wall, which also suggests that foot wall uplift is less than hanging wall subsidence. The folds close laterally as displacement decreases towards fault tips and offsets. It is not possible to detect a rollover on the cross-sections (Fig. 2) because the bed has been eroded northwards, and because there is no marked difference in bed dip in the hanging wall and the foot wall. The fault zone also shows 12 antithetic normal faults associated with uplift in the foot wall of the synthetic faults. They show up to about 90 mm aggregate displacement, compared with up to 400 mm displacement produced by synthetic segments. The hanging wall folds and antithetic faults in the foot wall appear to represent reverse drag (Barnett *et al.* 1987, Gibson *et al.* 1989). It is possible that the two antithetic faults at the main offset may be caused by rotation at the relay ramp.

Gibson *et al.* (1989) show that hanging wall subsidence (e.g. rollover) equals foot wall uplift for blind faults. However, the greater reorientation of hanging wall contours and the small size of the antithetic foot wall faults suggest that hanging wall subsidence exceeds foot wall uplift; this may be caused by the fault cutting the topographic surface (Gibson *et al.* 1989). However, it is possible that the contour pattern may be effected by pre-faulting variations in bed dip. Evidence for this includes a possible continuation of the hanging wall contour pattern beyond the east tip of the fault zone, the differences in the contour patterns near the east and west tips and the apparently greater amount of hanging wall subsidence in relation to foot wall uplift (J. Walsh personal communication 1990).

r/d_{MAX} *data for fault segments*

Figure 5 shows a logarithmic graph of r against d_{MAX} for the Kilve fault zone (where r = distance from the point of maximum displacement to the fault tip, and d_{MAX} = maximum displacement). r is used instead of the *radius* of Barnett *et al.* (1987) because the point of maximum displacement is often not at the centre of the fault trace. Data for British coalfield faults (Walsh & Watterson 1987, table 1) have also been plotted; these

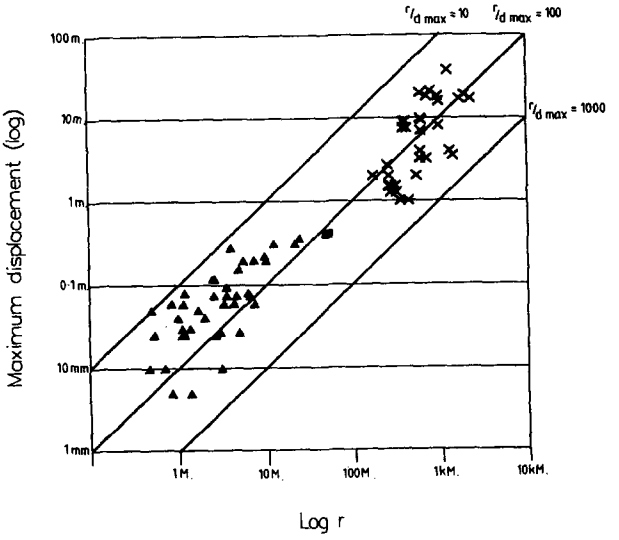

Fig. 5. Logarithmic (base 10) graph of r against d_{MAX} where r = the distance between the fault tip and the point of maximum displacement, and d_{MAX} = the maximum displacement. Square = whole fault zone. Triangles = segments at Kilve. Crosses = British coalfield data of Walsh & Watterson (1987). The Kilve segments tend to have lower r/d_{MAX} ratios than the whole fault zone and the coalfield data.

have an average r/d_{MAX} ratio of 142.7 (maximum of 440 and a minimum of 30), which is close to the ratio for the whole fault zone at Kilve ($r/d_{MAX} \approx 140$, $r \approx 55$ m from the east tip, $d \approx 0.4$ m). These data for isolated faults tend to be higher than the ratios for fault segments, with 43 r/d_{MAX} ratios for segments having a mean of 65.3; synthetic faults have a mean ratio of 51.5, whilst antithetic faults have a mean ratio of 88.5. The lowest ratio ($r/d_{MAX} = 10$) is for a synthetic fault, whilst the highest ratio ($r/d_{MAX} = 306.7$) is for an antithetic fault.

DISPLACEMENTS ALONG INDIVIDUAL SEGMENTS

Normalized displacement–distance data for the Kilve fault zone are shown in Fig. 6(a). There is a considerable scatter, well illustrated by variations for individual fault segments (Fig. 6b). The displacement characteristics of faults (i.e. brittle or discontinuous deformation) can be considered, and the variability in d–x data explained, both in terms of displacements along individual segments and displacements along linked segments. The ductile (continuous) deformation which occurs between offset faults tends to smooth out d–x profiles when added to fault displacement.

Models for the displacement characteristics of isolated faults

Various models exist for the displacement profiles of isolated faults. The simplest concerns a crack of length $2c$ subject to mode III (anti-plane shear) loading. Displacement has an elliptical form:

$$d = A(c^2 - x^2)^{1/2}, \quad (1)$$

where A is a constant dependant on the driving stress and on the elastic properties of the rock, c is the crack half length and x is the distance from the crack centre (e.g. Pollard & Segall 1987). Maximum displacement (d_{MAX}) occurs at the crack centre ($x = 0$), and is proportional to crack length. It is convenient to define normalized displacement ($D = d/d_{MAX}$) and distance ($X = x/c$), where both D and X vary from 0 to 1. Equation (1) then reduces to a circle:

$$D = (1 - X^2)^{1/2}. \quad (2)$$

The D–X data for the Kilve fault segments generally lie below this curve (Fig. 6a). Note that capital letters are used to denote normalized values of displacement and distance.

Walsh & Watterson (1987) suggest that faults are the result of a number of slip events. Their cumulative-slip model assumes that a propagating isolated planar fault accumulates slip increments according to the elastic model, the amount of incremental slip being proportional to fault length. They predict the D–X relationship:

$$D = 2(1 - X)\,(((1 + X)/2)^2 - X^2)^{1/2}. \quad (3)$$

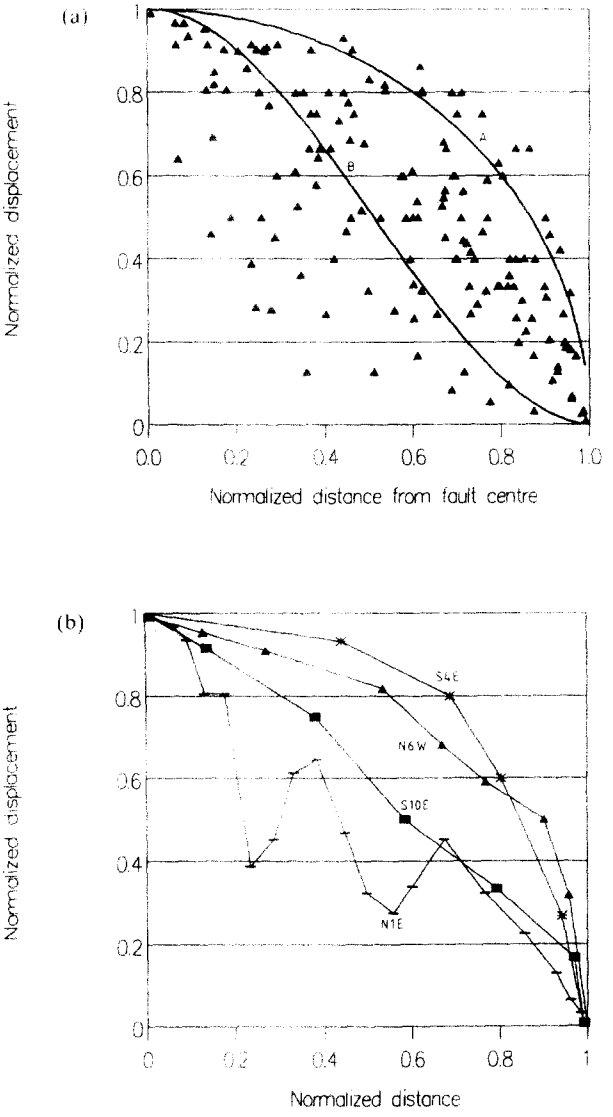

Fig. 6. (a) Normalized D–X data for Kilve fault segments (triangles), consisting of 245 data points along 44 fault radii from 29 segments. Profiles for the single-event elastic model (curve A) and the Walsh & Watterson (1987) cumulative-slip model (curve B) are also shown. (b) Examples of D–X plots for individual fault segments: S4(E) = connected fault. N6(W) = offset fault. S10(E) = nearly isolated fault. N1(E) = complex fault, composed of linked segments.

This profile approximates to the linear *C-type d–x* profile of Muraoka & Kamata (1983). The displacements at Kilve were measured along traces, through homogeneous limestone, and the linear profile derived for more isolated faults (Fig. 7) support the view of Muraoka & Kamata that such profiles are typical of homogeneous material.

Model for displacements along offset segments

Many of the segments in the fault zone at Kilve are not isolated, being offset and linked, and transferring displacement from one segment to another through a relay structure. Interference with other faults (Muraoka & Kamata 1983, Chadwick 1986, Ellis & Dunlap 1988,

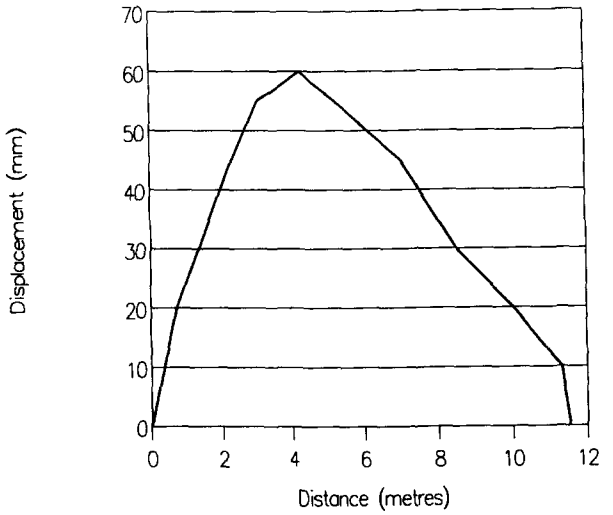

Fig. 7. Example of a linear displacement–distance graph (fault S10).

Larsen 1988, Walsh & Watterson 1989a,b), and related antithetic and synthetic faults (Gibson *et al.* 1989) can affect *d–x* profiles.

It is possible to model the *d–x* characteristics of offset segments (e.g. line 1, Fig. 8). For simplicity, it is assumed that an isolated fault has a linear *d–x* profile (line 2, Fig. 8), which approximates to the Walsh & Watterson (1987) cumulative-slip profile. It is also assumed that the *d–x* profile of an offset segment consists of two straight line portions, one between the point of maximum displacement and the start of the relay structure (portion A), and another between the start of the relay structure and the fault tip (portion B). Portions A and B intersect on a *D–X* graph (Fig. 8) at distance p, which has displacement q. Portion B is steeper because displacement is being transferred to the adjacent fault segment. Propagation is arrested at offset tips, where the displacement gradient increases, thus producing data that plots above the Walsh & Watterson profile (Figs. 6 and 8). The line 1 in Fig. 8 can result from the progressive steepening of the displacement gradient at the offset tip of an initially linear profile (line 2, Fig. 8). This model is a simplification because some fault propagation may occur (i.e. p may vary). The resultant profile may resemble that of an ideal single event elastic fracture (for instance, when p and q are both at about 0.7), and is often similar to the *M-type* profile of Muraoka & Kamata (1983) which has a flat central portion and steeply sloping flanks.

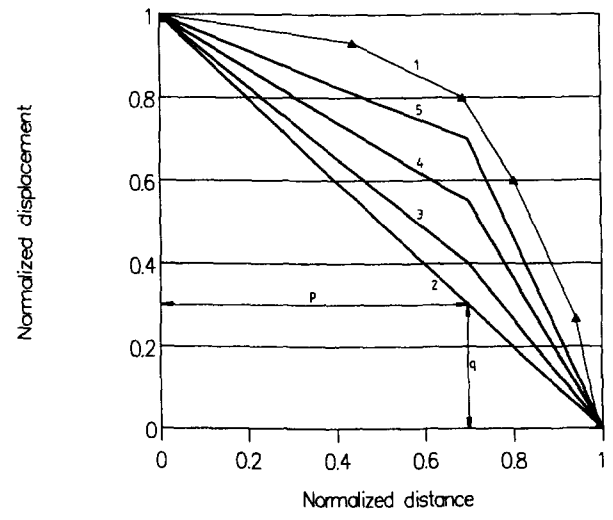

Fig. 8. 1 = segment S4E, which is an example of an offset fault segment with a *D–X* profile which plots above the Walsh & Watterson (1987) cumulative-slip profile (Fig. 6, curve B). 2 = linear (C-type) *D–X* profile. 3–5 = *D–X* plots of a developing fault segment with $p = 0.7$. 3 has $q = 0.4$, 4 has $q = 0.55$, 5 has $q = 0.7$. (See text for details.)

Offset faults tend to show higher displacement gradients at their tips than shown by isolated faults (Walsh & Watterson 1989a), which probably reduces the r/d_{MAX} ratio (Fig. 5). The smaller r/d_{MAX} ratios for the synthetic faults probably reflect their greater displacements and linkage compared to the antithetic faults.

RELAY STRUCTURES AND DISPLACEMENT TRANSFER

Aydin & Nur (1985) describe stepovers (offsets) in strike-slip faults, and distinguish between along-strike stepovers (offset in map view) and down-dip stepovers (offset in cross-section). A more general classification for offsets applicable to all fault classes would be displacement-parallel offsets (A in Fig. 9), displacement-normal offsets (B in Fig. 9, as at Kilve) and displacement-oblique offsets. Displacement-parallel offsets and displacement-oblique offsets can be further subdivided into those which are contractional (restraining) and extensional (releasing).

A *relay structure* may be defined (following Larsen 1988) as a zone connecting the foot wall and hanging wall of a fault zone, where displacement is transferred between offset segments. The reorientation of bedding at the offset often produces a *relay ramp*, which accommodates displacement transfer from one segment to another, whilst maintaining continuity between the foot wall and hanging wall (Fig. 9). The *relay structure* of Larsen (1988) appears to be the same as the *transfer zone* of Chadwick (1986) and the *fault bridge* of Ramsay & Huber (1987).

Connecting faults may cut the ramp to transfer displacement between segments. An alternative to relay structures are transfer faults (described by Gibbs 1984), which have strike-slip components, and trend at high angles to the offset normal faults which they link. Although Larsen (1988) discusses relay ramps in terms of offset listric faults with a common detachment, there is no need for the offset segments to be listric or connected; a relay can form between two separated planar normal faults (Fig. 9).

Study of the Kilve fault zone suggests that there is a relationship between the geometry of the relay ramp and the displacement variations along adjacent fault segments. Consider a schematic diagram of a relay structure (Fig. 10), in which two faults of equal maximum displacement overlap. The change in elevation between the hanging wall and foot wall, and the maximum throw on

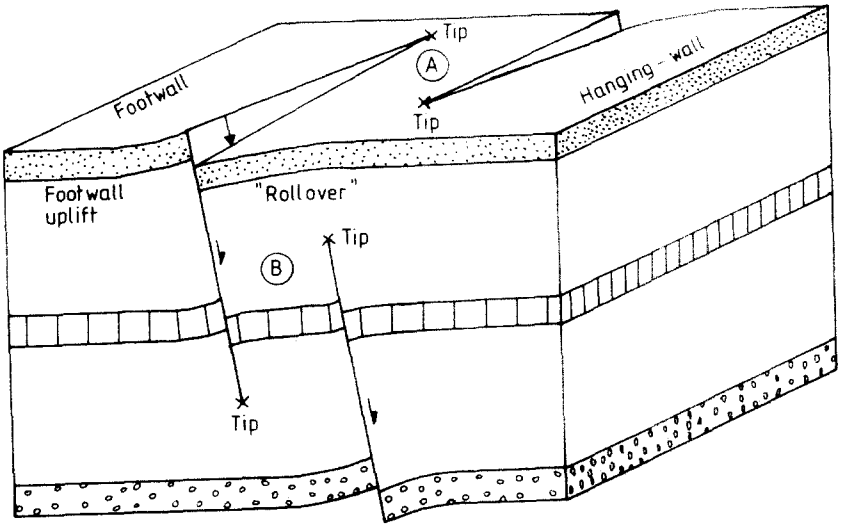

Fig. 9. Block diagram of a displacement-normal offset (A) and a displacement-parallel offset (B). Displacement-parallel offsets are visible in cross-sections of dip-slip faults or map views of strike-slip faults, whilst displacement-normal offsets are visible in map views of dip-slip faults or cross-sections of strike-slip faults.

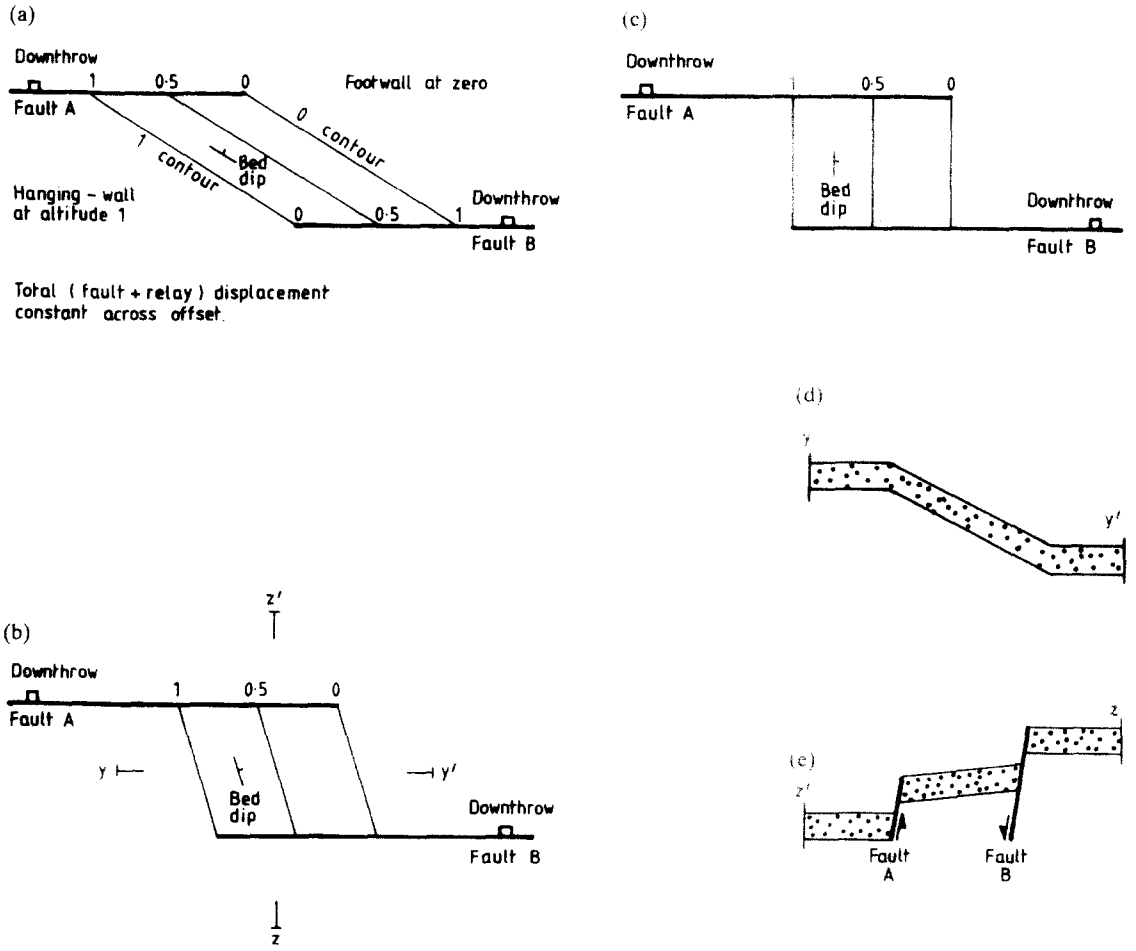

Fig. 10. Schematic diagram to show the form of a relay between two faults with varying overlap. Simplifications are made so that fault displacement away from the relay is constant, fault displacement decrease is constant at the relay, and there is no closure of wallrock structures at the relay. The strike and dip of the relay ramp is related to the degree of overlap and displacement gradients of the segments; as overlap increases, the ramp strike has a greater angle to the faults. (a) Offset at an early stage, with overlap not yet developed. (b) Overlap increasing, with relay rotation occurring. (c) Relay well developed, with ramp strike perpendicular to fault strike. (d) Cross-section y–y′ from (b), showing the vertical displacement transfer between offset faults caused by a relay ramp. (e) Cross-section z–z′ from (b), showing the decrease in vertical fault displacement caused by a relay ramp.

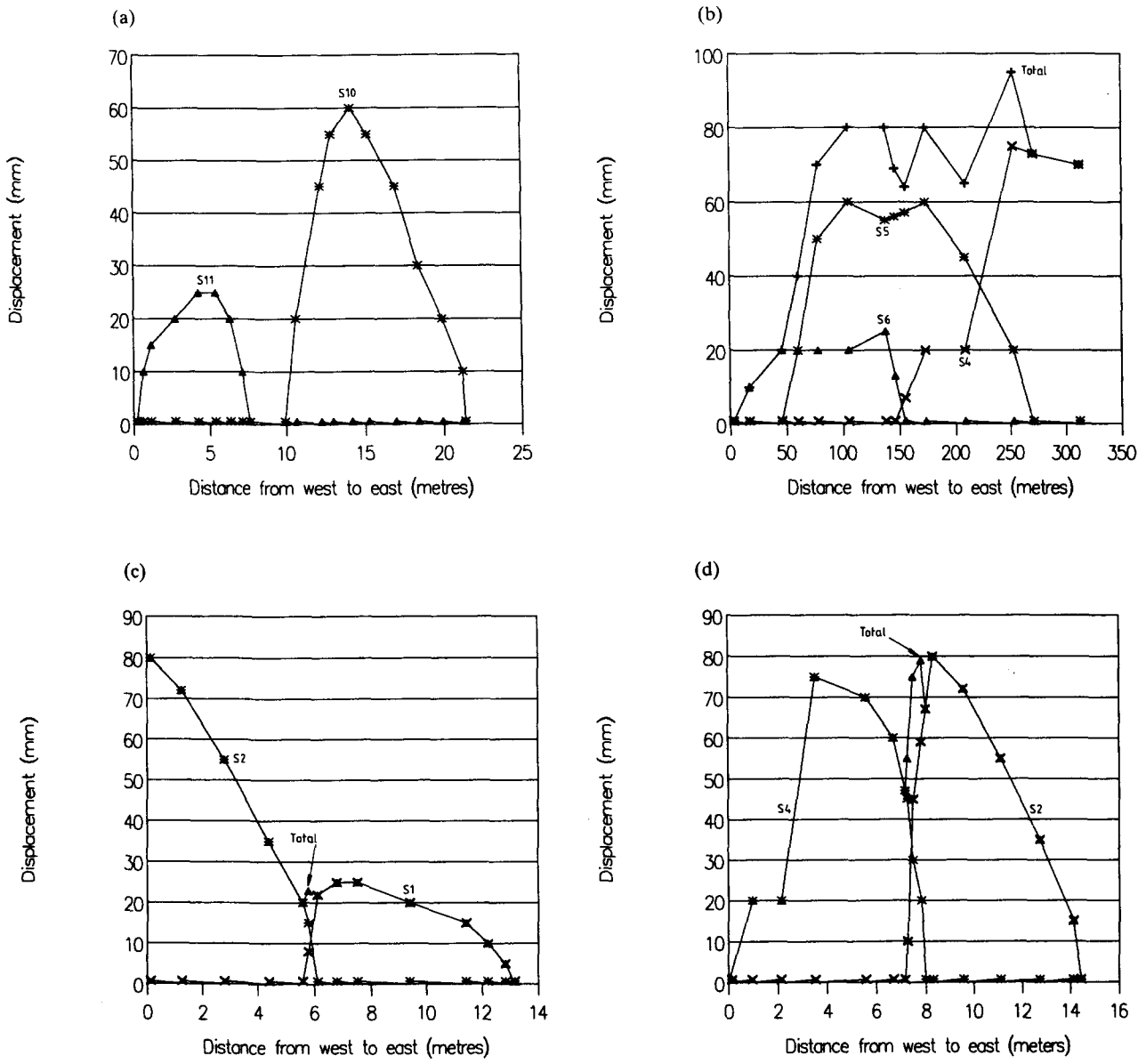

Fig. 11. Displacement–distance (d–x) graphs of offset and connected antithetic faults. (a) Faults S10 and S11; stage 1 offset with no overlap and each with a linear d–x profile. (b) Faults S4, S5 and S6; stage 2 offsets with total displacement having a d–x profile above the Walsh & Watterson (1987) cumulative-slip profile, but with displacement minima at offsets. (c) Faults S1 and S2; stage 2 offset. (d) Faults S2 and S4; stages 3–4 offset with displacement minima at the offset but an overall d–x profile above that of the cumulative-slip model.

each fault, is assigned one unit of height. The displacement gradients at the fault tips are constant. The relay ramp can be contoured by joining the 1-unit displacement point on fault A to the tip of fault B, and the x-unit point to the corresponding $1 - x$ point, etc. More irregular displacement gradients at the fault tips will produce more complex bends of the relay ramp. Figures 10 (a)–(c) show how the orientation of the relay ramp changes with the degree of overlap of the fault segments, and illustrates that major strike changes are to be expected. A section constructed parallel to the faults in Fig. 10(b) shows the apparent dip of strata in the relay ramp (Fig. 10d). This section represents the transfer of displacement between the offset segments. A cross-section normal to the faults (Fig. 10e) also shows an apparent dip of strata; this rotation of bedding partly accommodates the change in level from the hanging wall to the foot wall and thus accommodates the decrease in fault displacement at the offset (Figs. 11 and 12). Adding the continuous deformation to the discontinuous displacement tends to smooth out the d–x profiles of fault zones (Walsh & Watterson 1989a).

LINKAGE OF FAULT SEGMENTS

Evolution of normal fault zones

By examining the displacement characteristics of offset fault segments at Kilve, four stages in the development of normal fault zones may be postulated (Figs. 11 and 12). Figure 11 shows antithetic faults; the synthetic faults tend to show greater displacements and therefore more evolved and complex relays.

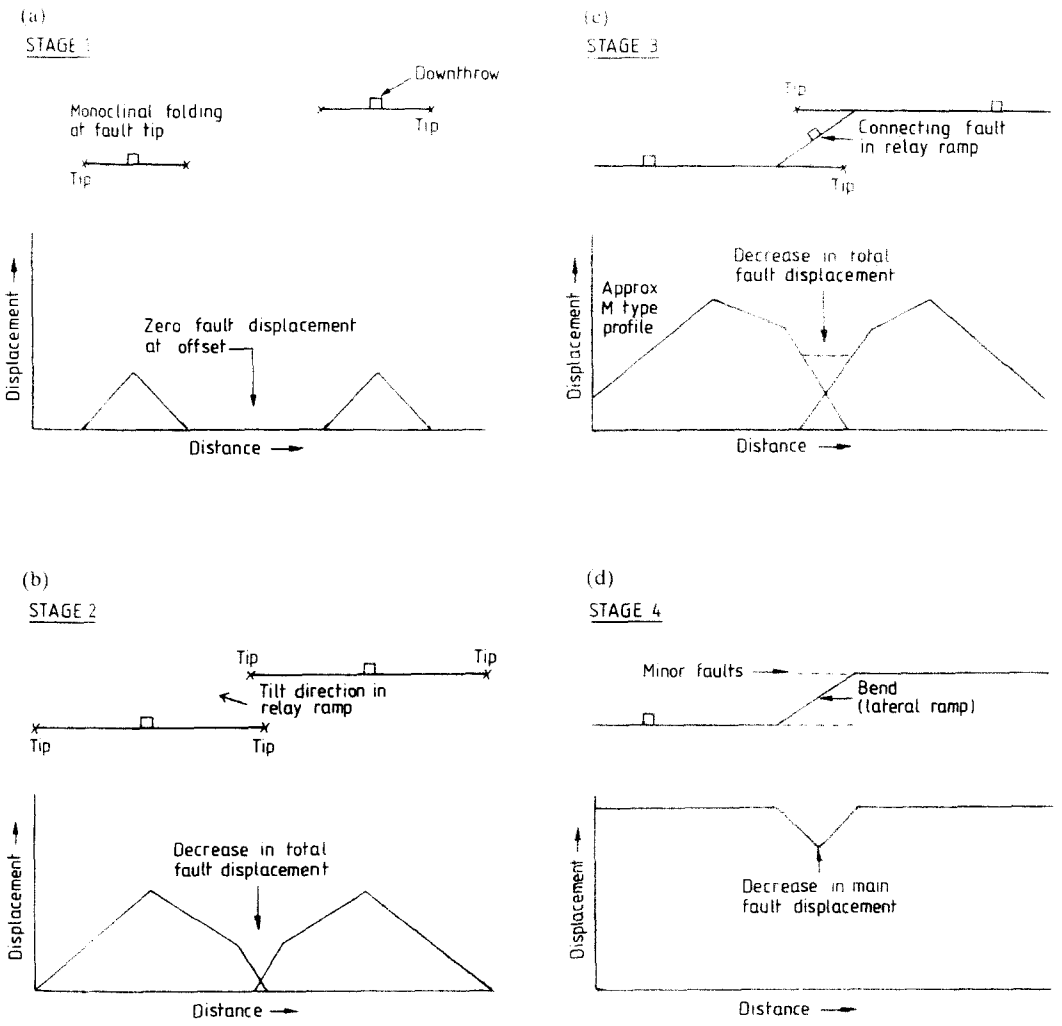

Fig. 12. Diagrams of stages of offset development, with corresponding displacement–distance graphs. (a) Stage 1; offset, underlapping faults. (b) Stage 2; overlap of faults, with displacement being transferred between the faults by rotation, and perhaps extension, of the relay ramp in a plane parallel to the faults. (c) Stage 3; the offset faults are linked by connecting faults, often producing rhomb-shaped fault blocks. (d) Stage 4; one connecting fault often becomes dominant, producing a fault bend which is approximately parallel to the displacement direction.

Stage 1 occurs where the fault segments do not overlap or interact, and the total fault displacement decreases to zero at the offset (Fig. 11a).

Stage 2 occurs where segments interact and displacement is transferred by relay structures (Figs. 11b & c). In Fig. 11(b), segments have profiles which plot above the Walsh & Watterson (1987) cumulative-slip profile because they have steep displacement gradients at offset tips. Total fault displacement is continuous and also plots above the cumulative-slip profile, but decreases at the offsets. Figure 11(c) also shows a decrease in total fault displacement at the offset, where again the faults show steeper gradients.

Stage 3 occurs where the relay ramp begins to be broken down by faults which link the segments (e.g. the main offset in Fig. 2).

Stage 4 (Fig. 11d) occurs where the offset segments are connected by a fault cutting the ramp, which is preserved as normal drag and causes a decrease in fault displacement at the connection. In Fig. 11(d), the individual segments have asymmetric linear d–x profiles, but the overall profile mostly plots above the cumulative-slip profile. Relay ramps can be destroyed as faulting continues, producing an *oblique* or *lateral transfer fault* (Larsen 1988) connecting the offset faults. Alternatively, with offset faults that are symmetrically arranged, relays can be destroyed as two faults propagate and join (Larsen 1988, fig. 3).

For offset fault segments, displacement decrease along one fault coincides with an increase along the other fault. However, as shown in Fig. 11 and by Walsh & Watterson (in press, figs. 14 and 15), there is often a decrease in total fault displacement, which may be taken up by either bending and tilting in the relay structures, or by folding of wallrocks. Each offset fault shows half-basin type subsidence in the hanging wall caused by a decrease in displacement towards the fault tips. The overlap of this folding causes a decrease in fault displacement at an offset. This is illustrated by the structure contours at the main offset (Fig. 2), where the small syncline may be an interference effect between the folds along the offset portions of the fault zone. Walsh & Watterson (1989a) point out that it is necessary to add continuous and discontinuous displacements, and

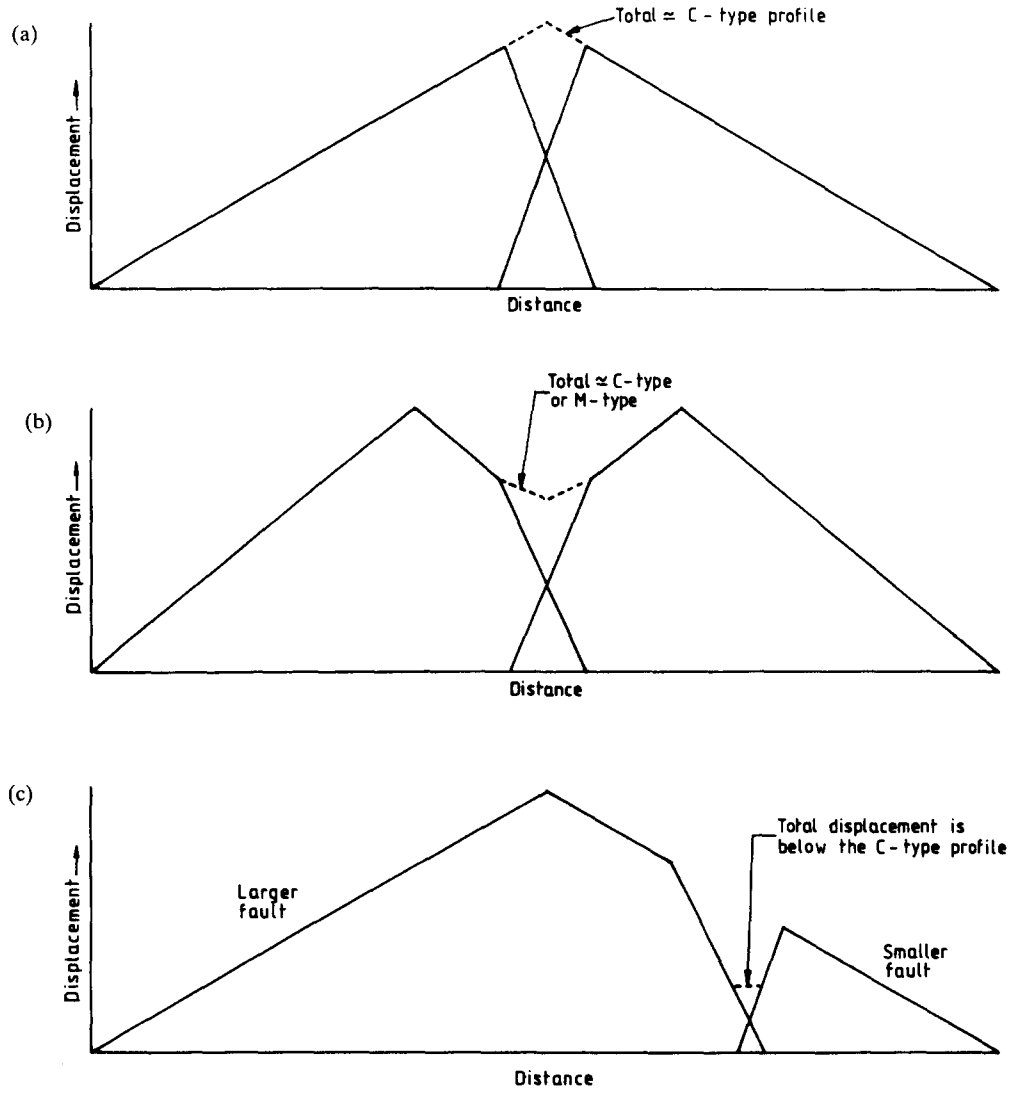

Fig. 13. (a) Displacement–distance (d–x) graph of fault initiation at or near the offset. (b) d–x graph of fault initiation away from the offset. (c) d–x graph of the linkage of two faults of different sizes.

suggest that the sum of displacements on an array of faults is comparable to the displacement on a single fault.

Effects of linkage on displacement profiles

Linkage may have two effects on the d–x graphs of offset or connected faults (Fig. 13), these being related to the relative sizes and points of maximum displacement of the segments. The first effect is where two segments of similar size link to produce a single fault with a d–x profile which plots above the Walsh & Watterson (1987) cumulative-slip profile (Figs. 13a & b). Examples of this include Figs. 11(b) and 14, and fig. 11 of Ellis & Dunlap (1988). The second effect involves the linkage of two differently sized fault segments (Fig. 13c) (also Walsh & Watterson in press, fig. 14). The combined fault will have a d–x profile with the maximum displacement near the centre of the larger segment, and a local minimum at the point of linkage, which may plot below the Walsh & Watterson profile. This may account for the large amount of data below that profile, both at Kilve (Fig. 6a) and for British coalfield data (Walsh & Watterson 1987, fig. 5), which Walsh & Watterson attribute to ductile drag. Figure 11(c) and fault S6 (Fig. 11b) may be examples of the type of d–x graph shown in Fig. 13(c). Ellis & Dunlap (1988) suggest that points of maximum displacement mark fault initiation points, and that displacement minima are points of linkage of fault segments and/or barriers along a single fault. The synthetic faults at Kilve tend to show more complex d–x profiles (e.g. fault N1 in Fig. 6b), and show a greater tendancy to plot below the cumulative-slip profile than the antithetic faults. This probably reflects their greater displacements and evolution.

Displacements along the whole fault zone

Figure 14 is a d–x graph of the whole fault zone, which is the sum of the displacements on the segments. Vertical displacement on the synthetic faults decreases at the main offset. Irregularities in the profile are largely the result of decreases in fault displacement at relay ramps. For example, the decrease in throw on the synthetic

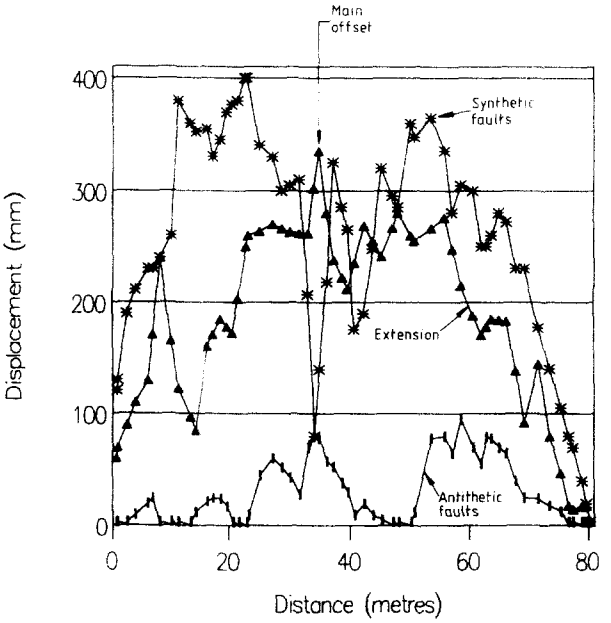

Fig. 14. Displacement–distance graph for the whole of the fault zone, showing a decrease in throw and increase in extension at the main offset.

faults east of the main offset is caused by the northward dip of bedding between the component faults; this may be a remnant of either fault-tip folding or a relay ramp. The measured extension (Fig. 14) shows a reasonably continuous d–x profile, with maximum extension occurring at the main offset. This may be due to either extension along the outer arc of the folded bed in the relay ramp (e.g. Ramsay & Huber 1987, fig. 21.18), or to increased extension in the transtensional offset (Sanderson & Marchini 1984).

CONCLUSIONS

Detailed mapping of a small normal fault zone at Kilve has revealed several features which may be typical of other fault zones, including faults with much greater displacements.

(1) The fault zone is made up from the displacement and linkage of many smaller segments, which have antithetic or synthetic displacements. Synthetic faults dominate, and antithetic faults appear to be related to bending at relay ramps and to foot wall uplift (reverse drag).

(2) Fault segments and zones show considerable variation in d–x graphs, with marked departures from the single event elastic model and the cumulative-slip model of Walsh & Watterson (1987). Reasons for this include the following.

(a) Individual offset segments tend to show convex-up d–x profiles caused by higher displacement gradients at offset tips.

(b) Offsets and linkage points are marked by decreases in fault displacement caused by the rotation of relay ramps and by the closure of wallrock structures.

(c) Linkage of segments causes complex slip/propagation relationships, tending to produce more concave-up d–x graphs than predicted by the Walsh & Watterson (1987) cumulative-slip model.

Much of the variation in d–x data, for individual segments and fault zones, may therefore be caused by varying fault slip/propagation relationships, and by the geometry of relay structures.

(3) Fault segments tend to have lower r/d_{MAX} ratios than isolated faults (where r = distance between the point of maximum displacement and the tip, and d_{MAX} = maximum displacement). Segments have higher displacement gradients at offset tips than do isolated faults (Walsh & Watterson 1989a), which probably reduces the r/d_{MAX} ratio.

(4) Relay structures can form between offset faults which may or may not be linked. Relays connect the foot wall with the hanging wall, and transfer displacement between offset faults. Relay structures and the closure of hanging wall structures cause a decrease in total fault displacement at an offset. However, fault displacement (discontinuous) plus relay ramp rotation (continuous deformation) is approximately constant across an offset.

(5) Four stages in the development of displacement-normal offsets can be identified.

Stage 1. Initial development of non-overlapping, non-interacting faults, each with an approximately linear d–x profile.

Stage 2. Overlap develops as the fault segments propagate towards each other, with displacement transfer occurring by means of a relay ramp, causing displacement gradients to increase at the offset tips.

Stage 3. Connecting fault(s) develops across the ramp.

Stage 4. The ramp is destroyed, producing a lateral ramp or transfer fault.

Acknowledgements—We are grateful to M. Ellis, S. Treagus and J. Walsh for their helpful reviews. D. Peacock received a research studentship from the Natural Environment Research Council. P. Durnford and J. Gully are thanked for their help in drafting the diagrams. G. Peacock helped map the fault zone.

REFERENCES

Aydin, A. & Nur, A. 1985. The types and role of stepovers in strike-slip tectonics. In: *Strike-slip Deformation, Basin Formation, and Sedimentation* (edited by Biddle, K. T. & Christie-Blick, N). *Spec. Publs Soc. econ. Palaeont. Miner.* **37**, 35–44.

Barnett, J. A. M., Mortimer, J., Rippon, J. H., Walsh, J. J. & Watterson, J. 1987. Displacement geometry in the volume containing a single normal fault. *Bull. Am. Ass. Petrol. Geol.* **71**, 925–937.

Beach, A. 1989. The geometry of normal faults—examples from the Jurassic of Somerset. *Abstract at the Geol. Soc. Lond. Meeting, The Geometry of Normal Faults*, 14–15 June.

Brooks, M., Trayner, P. M. & Trimble, T. J. 1988. Mesozoic reactivation of Variscan thrusting in the Bristol Channel area, U.K. *J. geol. Soc. Lond.* **145**, 439–444.

Chadwick, R. A. 1986. Extension tectonics in the Wessex Basin, southern England. *J. geol. Soc. Lond.* **143**, 465–488.

Donato, J. A. 1988. Possible Variscan thrusting beneath the Somerton Anticline, Somerset. *J. geol. Soc. Lond.* **145**, 431–438.

Ellis, M. A. & Dunlap, W. J. 1988. Displacement variation along thrust faults: implications for the development of large faults. *J. Struct. Geol.* **10**, 183–192.

Gibbs, A. D. 1984. Structural evolution of extensional basin margins. *J. geol. Soc. Lond.* **141**, 609–620.

Gibson, J. R., Walsh, J. J. & Watterson, J. 1989. Modelling of bed contours and cross-sections adjacent to planar normal faults. *J. Struct. Geol.* **11**, 317–328.

King, G. C. P. 1983. The accommodation of large strains in the upper

lithosphere of the earth and other solids by self-similar fault systems: the geometric origin of b-value. *Pure & Appl. Geophys.* **121**, 761–1091.

King, G. C. P. 1986. Speculations on the geometry of the initiation and termination processes of earthquake rupture and its relation to morphology and geological structure. *Pure & Appl. Geophys.* **124**, 567–585.

Larsen, P.-H. 1988. Relay structures in a Lower Permian basement-involved extension system, East Greenland. *J. Struct. Geol.* **10**, 3–8.

McLachlan, A. C. 1986. A revised interpretation of the structures within the Mesozoic of north-west Somerset. Unpublished M.Sc. thesis, Imperial College, London.

Muraoka, H. & Kamata, H. 1983. Displacement distribution along minor fault traces. *J. Struct. Geol.* **5**, 483–495.

Peacock, D. C. P. 1990. Displacement transfer at fault offsets and bends. Unpublished Ph.D. thesis, University of Southampton, U.K.

Pollard, D. D. & Segall, P. 1987. Theoretical displacements and stresses near fractures in rock: with applications to faults, joints, veins, dikes, and solution surfaces. In: *Fracture Mechanics of Rock* (edited by Atkinson, B. K.). Academic Press, New York, 277–349.

Ramsay, J. G. & Huber, M. I. 1987. *The Techniques of Modern Structural Geology, Volume* 2: *Folds and Fractures*. Academic Press, London.

Sanderson, D. J. & Marchini, W. R. D. 1984. Transpression. *J. Struct. Geol.* **6**, 449–458.

Walsh, J. J. & Watterson, J. 1987. Distributions of cumulative displacement and seismic slip on a single normal fault surface. *J. Struct. Geol.* **9**, 1039–1046.

Walsh, J. J. & Watterson, J. 1989a. Displacement gradients on fault surfaces. *J. Struct. Geol.* **11**, 307–316.

Walsh, J. J. & Watterson, J. 1989b. Kinematic coherence in normal fault systems. *Abstract at the Geol. Soc. Lond. Meeting, The Geometry of Normal Faults*, 14–15 June.

Walsh, J. J. & Watterson, J. In press. New methods of fault projection for coalmine planning. *Proc. Yorks. geol. Soc.*

Whittaker, A. & Green, G. W. 1983. *Geology of the Country Around Weston-Super-Mare*. Mem. Geol. Surv. G.B. Sheet 279 and parts of 263 and 295.